Atomic Radii for Continuum Electrostatics Calculations Based on Molecular Dynamics Free Energy Simulations

Mafalda Nina,[†] Dmitri Beglov,[‡] and Benoît Roux*[,†,‡]

Groupe de Recherche en Transport Membranaire (GRTM), Départements de physique et de chimie, Université de Montréal, C.P. 6128, succ. Centre-Ville, Canada H3C 3J7, and CERCA, Centre de Calcul en Recherche Appliquée, 5160, Boul. Decarie, Bureau 400, Montréal, Québec, Canada H3X 2H9

Received: February 27, 1997[⊗]

The electrostatic contribution to the solvation free energy of the 20 naturally occurring amino acids is examined using atomic models. The amino acids are modeled by *N*-acetyl-X-*N*′-methylamide. Free energy perturbation techniques with explicit water molecules are used to evaluate the contribution of solute−solvent electrostatic interactions to the solvation free energies. An analysis based on the radial solvent charge distribution yields a basic rule to determine a set of atomic Born radii defining the dielectric boundary between the solute and the solvent in continuum electrostatic models. Minor adjustments are made to refine the atomic Born radii in order to reproduce quantitatively the electrostatic contribution to the solvation free energy calculated by free energy perturbation techniques. The good agreement of continuum electrostatic and molecular dynamics free energy perturbations suggests that the new set of atomic Born radii may be used as a computationally inexpensive alternative to the microscopic treatment of solvent with explicit water molecules.

I. Introduction

Solvation effects provide the major force driving the conformational equilibrium, folding, and association of peptides, proteins, and other biomolecules.[1,2] In particular, the solvation free energy for peptides and proteins is dominated by electrostatics due to the polarity of the peptide backbone. The electrostatic contribution to the solvation free energy is on the order of 10 and 100 kcal/mol for polar and ionic residues, respectively.[3,4] Thus, it is important to develop computational methods able to account quantitatively for the electrostatic contribution to the solvation free energy of peptides and proteins.

From a rigorous point of view, the total solvation free energy of a solute molecule may be expressed as the reversible work for its materalization into the bulk solvent in a step-by-step process.[5] In particular, one can envision the solvation free energy of a solute as the total reversible work needed to create a neutral cavity into the solvent and, subsequently, include the van der Waals dispersion as well as the electrostatic interactions between the solute and the solvent molecules (see Scheme 1),

$$\Delta G = \Delta G_{\text{cavity}} + \Delta G_{\text{VDW}} + \Delta G_{\text{elec}} \qquad (1)$$

Although a free energy decomposition based on eq 1 is path-dependent,[6] it provides a useful and rigorous framework for understanding the different contributions to the solvation free energy and for constructing suitable approximations.

Computer simulations of atomic models in which water molecules are explicitely taken into account represent the most detailed method to study the influence of solvation.[7−10] Thermodynamic perturbation (TP) or thermodynamic integration (TI) methods[11] may be used with molecular dynamics simulations to artificially materialize a solute molecule in the solvent by varying one or more parameters such as the atomic radii and charges.[12] Nevertheless, these computationally intensive methodologies often suffer from statistical uncertainties due to finite sampling, and their applicability to very large systems such as proteins become prohibitive.[13−16] To represent implicity the influence of solvent on peptides and proteins, phenomenological solvent-accessible surface models have been proposed.[17−22] These approaches are computationally inexpensive and work quite well for nonpolar molecules.[23−26] However, such approximations only make sense if the interactions between the solute and the bulk solvent are of a short-range nature, since the shielding of intramolecular electrostatic interactions arising from the solvent reaction field is ignored. A description of the solvation based on macroscopic continuum electrostatics can overcome this limitation (see ref 27 for a recent review). This approximation, in which the polar solvent is represented as a structureless continuum dielectric medium, was originally pioneered by Born in 1920 to calculate the hydration free energy of spherical ions.[28] It was later extended by Kirkwood[29] to treat arbitrary charge distributions inside a spherical cavity. With the use of powerful computers, the treatment of solutes of arbitrary shape was made possible by solving the Poisson

SCHEME 1: Thermodynamic Cycle Showing the Decomposition of the Total Solvation Free Energy into Nonpolar and Electrostatic Contributions[a]

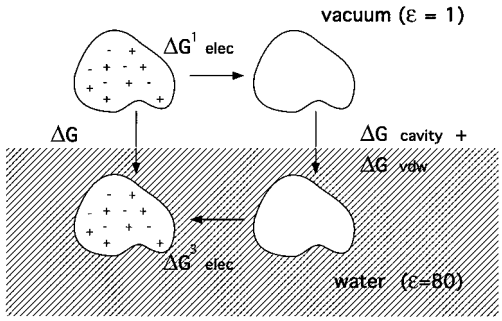

[a] ΔG is the total solvation free energy. $\Delta G_{\text{elec}} = \Delta G^1_{\text{elec}} + \Delta G^3_{\text{elec}}$ where ΔG^1_{elec} corresponds to the Coulombic term in a homogeneous medium and ΔG^3_{elec} to the total electrostatic contribution to the solvation free energy. The nonpolar contribution is the sum of $\Delta G_{\text{cavity}} + \Delta G_{\text{VDW}}$.

* To whom correspondence should be addressed. Telephone: (514) 343-7105. Fax: (514) 343-7586. E-mail: ROUXB@PLGCN.UMONTREAL.CA.
† Groupe de Recherche en transport membranaire.
‡ Centre de Calcul en Recherche Appliquée.
⊗ Abstract published in *Advance ACS Abstracts,* June 1, 1997.

S1089-5647(97)00736-0 CCC: $14.00

equation numerically with finite-difference algorithms:[30]

$$\nabla\cdot[\epsilon(\mathbf{r})\nabla\Psi(\mathbf{r})] = -4\pi\rho^{\text{solute}}(\mathbf{r}) \tag{2}$$

where $\Psi(\mathbf{r})$ is the total electrostatic potential, $\epsilon(\mathbf{r})$ is the position-dependent dielectric constant, and $\rho^{\text{solute}}(\mathbf{r})$ is the charge density due to the solute.

Numerical solution to the Poisson equation can provide a very effective approach for treating the influence of electrostatic solvent effects on molecules of arbitrary shape.[27,31] However, results obtained using macroscopic continuum electrostatics for peptides or proteins depend sensitively on the location of the dielectric boundary between the solute and the solvent. This is due to the fact that the surface charge density caused by the solvent polarization giving rise to the solvent reaction field is located at the dielectric discontinuity.[32] In seeking a rigorous basis for extending macroscopic continuum electrostatic models to larger molecular solutes, several studies examined the Born model from a microscopic point of view.[33−35] Simulations with explicit solvent showed that the properties of the water molecules close to the ion are very different from those of the bulk (see ref 33 and references therein). Yet, the Born model is remarkably successful in reproducing the solvation free energy of a large number of ions.[36] One reason for its quantitative accuracy was attributed to the cancellation of two opposing effects: dielectric saturation and electrostriction.[33] The electric field of the ion tends to lower the local dielectric constant (saturation), whereas the tendency of water molecules to crowd around the ion tends to increase the local dielectric constant of the solvent (electrostriction). It was shown that the ionic radius of hydration should be interpreted in terms of the first peak in the solute−solvent radial distribution function.[35] As a consequence, the optimal value for ionic radius is not a property of the ion alone but is an effective quantity depending on the charge of the ion and also on the molecules forming the bulk solvent.[35] For example, this is reflected in the difference in solvation free energy between anions and cations in bulk water due to the asymmetric structure of the water molecule.[33−36] To effectively take into account the microscopic solvent structure, the ionic radius in the Born model should be considered as an empirical parameter.[34,36] Similarly, the parametrization of the continuum model for peptides and proteins involves the development of an optimal set of atomic radii, effectively a generalization for molecular solutes of the ionic Born radius. Different parametrizations have been proposed to reproduce experimental and theoretical solvation free energies. For a number of small molecules, atomic radii (and charges) have been optimized from existing force fields to be in accord with experimental data, and results from numerical solution of the Poisson equation have been compared to free energy simulations with explicit water molecules.[24,37−42] Nevertheless, despite these efforts, there is still no consensus on an optimal set of atomic radii for peptides and proteins continuum electrostatic calculations.

The goal of the present article is to develop an optimal set of "atomic Born radii" for continuum electrostatic calculations consistent with the results of molecular dynamics free energy simulations of peptides and proteins with explicit water molecules. In section II, a microscopic description of the electrostatic contribution to the solvation free energy with an explicit model of the solvent is related to continuum electrostatics in terms of the solvent charge distribution. Microscopic systems, *N*-acetyl-X-*N*′-methylamide $CH_3-CO-NH-CR-CO-NH-CH_3$, modeling the protein backbone and side chains are presented in section III. Computational methods used in calculations of radial solvent charge distribution functions and details of thermodynamic perturbation and continuum electrostatics calculations are also given. Section IV presents the results and discussion. The procedure used to determine the atomic radii is described. Electrostatic contributions to the solvation free energies using explicit and continuum models of the solvent are given. Summary and conclusion are presented in section V.

II. Theory

Microscopic Description and Relation to Continuum Electrostatic. To make progress in determining an optimal set of atomic radii, it is useful to revisit the microscopic basis of the continuum electrostatic approximation. A solute molecule immersed in bulk water at a fixed position is considered. It is assumed that the molecule is nonpolarizable and the dielectric constant of the microscopic model is $\epsilon = 1$. The electrostatic contribution to the free energy difference between two states of the solute molecule, i.e., fully charged ($\lambda = 1$) and zero-charged ($\lambda = 0$) is

$$\Delta G_{\text{elec}} = \int_0^1 \mathrm{d}\lambda \left\langle \frac{\partial U(\lambda)}{\partial \lambda} \right\rangle_{(\lambda)} \tag{3}$$

where $U(\lambda) = \lambda U_1 + (1 - \lambda)U_0$ refers to the solute−solvent interaction energy for any value of the coupling parameter λ in the interval [0,1], U_0 is the potential energy of the solute−solvent system with atomic charges of the solute set to zero, and U_1 is the potential energy when the solute is fully charged. Equation 3 can be evaluated using free energy perturbation methods with explicit solvent−solute molecules. Since the perturbed term involved in the reversible work for charging the solute is the Coulombic term, ΔG_{elec} is given by

$$\Delta G_{\text{elec}} = \int_0^1 \mathrm{d}\lambda \left\langle \sum_{i,j} \frac{q_i q_j}{|\mathbf{r}_i - \mathbf{r}_j|} \right\rangle_{(\lambda)} \tag{4}$$

where q_i and q_j are, respectively, the solute and the solvent atomic charges of atoms i and j and $\mathbf{r}_i$ and $\mathbf{r}_j$ describe the atomic charge positions

$$\Delta G_{\text{elec}} = \int_0^1 \mathrm{d}\lambda \sum_i q_i \left\langle \sum_j q_j \frac{1}{\mathbf{r}_i - \mathbf{r}_j|} \right\rangle_{(\lambda)} \tag{5}$$

Since the solute atom positions $\mathbf{r}_i$ are fixed and only the bulk water molecules positions $\mathbf{r}_j$ are allowed to vary,

$$\Delta G_{\text{elec}} = \int_0^1 \mathrm{d}\lambda \sum_i q_i \int \mathrm{d}\mathbf{r} \frac{1}{|\mathbf{r}_i - \mathbf{r}|} \langle \rho_{\text{elec}}(\mathbf{r}) \rangle_{(\lambda)} \tag{6}$$

where $\langle \rho_{\text{elec}}(\mathbf{r}) \rangle_{(\lambda)}$ is the average radial solvent charge distribution function

$$\langle \rho_{\text{elec}}(\mathbf{r}) \rangle_{(\lambda)} = \langle \sum_j q_j \, \delta(\mathbf{r}_j - \mathbf{r}) \rangle_{(\lambda)} \tag{7}$$

The solvent reaction field acting at the position of the ith solute partial charge is

$$\langle \Psi_{\text{rf}}^{(i)} \rangle_{(\lambda)} = \int \mathrm{d}\mathbf{r} \frac{1}{|\mathbf{r}_i - \mathbf{r}|} \langle \rho_{\text{elec}}(\mathbf{r}) \rangle_{(\lambda)} \tag{8}$$

Equivalently, the solvent reaction field may be expressed in terms of the average radial solvent charge distribution around

the solute ith atom $\langle\rho_{\mathrm{elec}}^{(i)}(r)\rangle_{(\lambda)}$:

$$\langle\Psi_{\mathrm{rf}}^{(i)}\rangle_{(\lambda)} = 4\pi\int_0^\infty r^2\,\mathrm{d}r\,\frac{1}{r}\langle\rho_{\mathrm{elec}}^{(i)}(r)\rangle_{(\lambda)} \tag{9}$$

Finally, the total charging free energy is

$$\Delta G_{\mathrm{elec}} = \int_0^1 \mathrm{d}\lambda \sum_i q_i \langle\Psi_{\mathrm{rf}}^{(i)}\rangle_{(\lambda)} \tag{10}$$

In continuum macroscopic electrostatics, the average solvent charge distribution function around the solute is[43]

$$\langle\rho_{\mathrm{elec}}(\mathbf{r})\rangle = -\nabla\cdot\mathbf{P}(\mathbf{r}) \tag{11}$$

where $\mathbf{P}(\mathbf{r})$ is the average polarization density of the solvent. Based on the assumption that at any point $\mathbf{r}$ the polarization $\mathbf{P}(\mathbf{r})$ and the total electrostatic field $\mathbf{E}^{\mathrm{tot}}(\mathbf{r})$ are linearly related, $\mathbf{P}(\mathbf{r})$ is given by

$$\mathbf{P}(\mathbf{r}) = \left(\frac{\epsilon(\mathbf{r})-1}{4\pi}\right)\mathbf{E}^{\mathrm{tot}}(\mathbf{r}) \tag{12}$$

where $\epsilon(\mathbf{r})$ is the position-dependent dielectric constant. To describe the dielectric constant in the solute and in the solvent, $\epsilon(\mathbf{r})$ can be expressed as $\epsilon(\mathbf{r}) = 1 + \theta(\mathbf{r})(\epsilon_{\mathrm{bulk}} - 1)$, where

$$\theta(\mathbf{r}) = \begin{cases} 0 & \text{inside the solute} \\ 1 & \text{outside the solute.} \end{cases} \tag{13}$$

Because eq 12 is linear, the thermodynamic integration corresponding to the reversible work done during the charging process is

$$\Delta G^{\mathrm{Poisson}} = \frac{1}{2}\sum_i q_i \langle\Psi_{\mathrm{rf}}^{(i)}\rangle_{(\lambda=1)} \tag{14}$$

Since the divergence of the polarization density is zero except at the dielectric boundary,[43] the solvent charge density corresponds to a sharply peaked function localized at the solute−solvent interface and

$$\langle\rho_{\mathrm{elec}}(\mathbf{r})\rangle = \left(\frac{\epsilon_{\mathrm{bulk}}-1}{4\pi}\right)\mathbf{E}^{\mathrm{tot}}(\mathbf{r})\cdot\nabla\theta(\mathbf{r}) \tag{15}$$

where $\nabla\theta(\mathbf{r})$ is a delta function pointing in the direction of the normal at the solute surface. This analysis shows that an important concept in relating the continuum model to a microscopic description is the average solvent charge distribution function. This relation will be exploited in deriving the set of atomic radii for peptides and proteins.

The results obtained using the continuum electrostatic approximation depend critically on the location of the dielectric boundary between the solute and the solvent (see eq 15 above). The Born model of hydration[28] for the electrostatic solvation energy of a single spherical ion provides a useful framework to illustrate the approximation involved in the determination of the dielectric boundary for macroscopic continuum electrostatic approximation. In the Born model, the excess chemical potential is a function of the charge of the ion Q_{ion}, the radius R_{ion}, and the dielectric constant of the solvent ϵ:

$$\Delta G_{\mathrm{elec}} = \frac{{Q_{\mathrm{ion}}}^2}{2R_{\mathrm{ion}}}\left(\frac{1}{\epsilon}-1\right) \tag{16}$$

This expression, corresponding to the reversible electrostatic work necessary to charge an ion in a continuum dielectric solvent, can be easily derived. In continuum electrostatic, the solvent charge density is sharply peaked at the solute−solvent boundary and the solvent reaction field is approximately (see eq 9)

$$\langle\Psi_{\mathrm{rf}}\rangle_{(\lambda)} \approx \frac{1}{R_{\mathrm{ion}}}4\pi\int_0^\infty r^2\,\mathrm{d}r\,\langle\rho_{\mathrm{elec}}(r)\rangle_{(\lambda)} \tag{17}$$

where the remaining integral on the left-hand side corresponds to the total average solvent charge density distribution function around the ion. According to Gauss's theorem for a charge λQ_{ion} in a medium of dielectric constant ϵ, the total charge density obeys the sum rule[35]

$$4\pi\int_0^\infty r^2\,\mathrm{d}r\,\langle\rho_{\mathrm{elec}}(r)\rangle_{(\lambda)} = \lambda Q_{\mathrm{ion}}\left(\frac{1}{\epsilon}-1\right) \tag{18}$$

and the reaction field is (in the continuum limit)

$$\langle\Psi_{\mathrm{rf}}\rangle_{(\lambda)} \approx \frac{1}{R_{\mathrm{ion}}}\lambda Q_{\mathrm{ion}}\left(\frac{1}{\epsilon}-1\right) \tag{19}$$

Since the solvent reaction field is linearly proportional to the coupling parameter (linear response), the thermodynamic integration yields a factor of one-half. As shown by eq 17, the magnitude of the free energy is very sensitive to the position of the solute−solvent boundary (i.e., the size of R_{ion}). In the continuum limit, the charge density is completely concentrated at the solute−solvent boundary, R_{ion}. This implies that the reaction field results from the solvent charge within an infinitesimal layer of thickness δ

$$\langle\Psi_{\mathrm{rf}}\rangle = 4\pi\int_{R_{\mathrm{ion}}-\delta}^{R_{\mathrm{ion}}+\delta} r^2\,\mathrm{d}r\,\frac{1}{r}\langle\rho_{\mathrm{elec}}(r)\rangle \tag{20}$$

In contrast, the solvent charge density in an atomic model is distributed over a microscopic region of space of finite dimension. The size of this microscopic region has important consequences on the reaction field at the center of a spherical cavity and, thus, on the solvation free energy. The dependence of the ionic radius on the sign of an ion is illustrated for microscopic models of K^+ and Cl^-. The Lennard-Jones parameters of the ions were adjusted to yield the same solvation free energy in bulk water, −80 kcal/mol (details are given in ref 44).

To examine the physical thickness attributed to the solvent charge density, we define the quantity

$$\langle\Psi_{\mathrm{rf}}(R)\rangle = 4\pi\int_0^R r^2\,\mathrm{d}r\,\frac{1}{r}\langle\rho_{\mathrm{elec}}(r)\rangle \tag{21}$$

which is the reaction field potential due to the solvent within a shell of radius R around the ion. The average radial solvent charge distribution function for K^+ and Cl^- is shown in Figure 1a. The solvent reaction field $\langle\Psi_{\mathrm{rf}}(R)\rangle$ is shown in Figure 1b. The magnitude of the reaction field appears dramatically different for K^+ and Cl^- close to the ion and then becomes similar (with opposite sign) for distances larger than 5 Å. However, the Born radius R_{ion} must be the same for K^+ and Cl^-, since they have the same electrostatic free energy as designed. If the continuum electrostatic approximation was exact, the reaction field of K^+ and Cl^- would jump abruptly to their limiting value at $R_{\mathrm{ion}} = 2$ Å. For quantitative accuracy, it is possible to choose the value of the Born ionic radii to reproduce the free energy of charging, although this does not bear much resemblance to the average microscopic solvent structure around the ions. It is clear by considering Figure 1a that the average solvent charge distribution is quite different for the two ions and that the significance of a precise value for

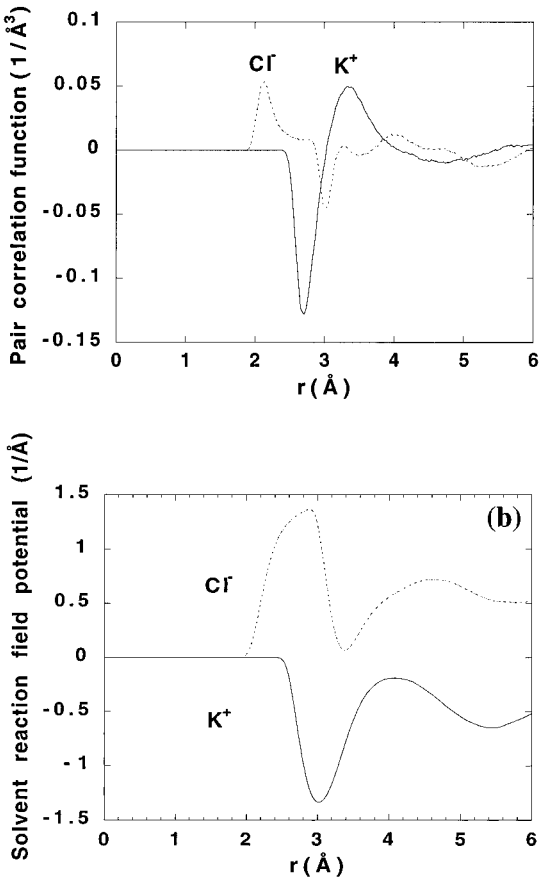

Figure 1. Solvation of Cl^- and K^+ in bulk water. Part a shows the average radial solvent charge distribution $\langle \rho_{elec}(r) \rangle$ around the two ions. The average structure of the solvent around the ions was calculated from molecular dynamics trajectories of 200 ps of Lennard-Jones models of K^+ and Cl^- in a sphere of 120 TIP3P molecules submitted to a spherical solvent boundary potential (SSBP).[49] Part b shows the integrated solvent reaction field potential $\langle \Psi_{rf}(R) \rangle$ calculated on the basis of eq 21.

the Born radii is limited by the spatial extent of the average solvent charge density. More generally, the atomic radii used to construct the solute−solvent dielectric boundary should be viewed as an idealization that requires some empirical adjustments. The final goal is to have a continuum electrostatic model with quantitative accuracy relative to molecular dynamics simulations with explicit solvent molecules. The continuum electrostatic model has a sound physical basis and corresponds to a well-defined limit.[45] However, the microscopic correlation length of the solvent is larger than the small adjustments that are made on the value of the atomic Born radii.

III. Microscopic Systems and Computational Methods

Microscopic Systems. The nonzwitterionic tripeptide *N*-acetyl-X-*N*′-methylamide ($CH_3-CO-NH-CR-CO-NH-CH_3$) was choosen as a model of the protein backbone (Figure 2a). X is Gly, Ala, Val, Ile, Leu, Phe, Tyr, Cys, Trp, Arg, Glu, Asp, Lys, Thr, Pro, Met, Ser, His, Asn, and Gln (R is the corresponding side chain). Atom types as found in all-hydrogen PARM22 parameters file are shown in Figure 2b. Asp and Glu side chains were deprotonated, His is neutral (protonated on ND1), and Lys and Arg were protonated in these calculations. The all-hydrogen PARM22 potential function of CHARMM[46] was used. Initial side chains conformations of all amino acids were obtained from a backbone-independent rotamer library corresponding to the most frequent conformations found in proteins[47] (see Table 1). The backbone ϕ and ψ dihedral angles

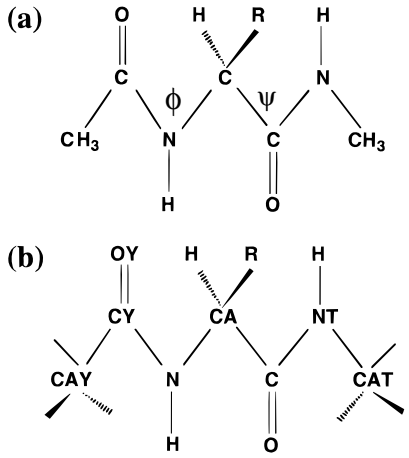

Figure 2. (a) Schematic diagram of the tripeptide *N*-acetyl-X-*N*′-methylamide, $CH_3-CO-NH-CR-CO-NH-CH_3$, chosen as a model of the protein backbone. R is the side chain group of the 20 amino acids. ϕ and ψ dihedral angles are indicated in an extended conformation as considered in the calculations. (b) Atom types are indicated as found in the all-hydrogen PARM22 parameters file.

TABLE 1: Backbone-Independent Rotamer Library for All Standard Amino Acids, from Dunbrack et al.[45,a]

residues	χ_1	χ_2	χ_3	χ_4
Val	180			
Leu	−60	180 (−148)		
Ile	−60	180		
Pro	30 (32)	−30 (34)		
Phe	−60 (−65)	90 (97)		
Trp	−60	90		
Met	−60	180		
Ser	60			
Thr	60			
Cys	−60			
Tyr	−60	90		
Asn	−60 (−125)	−60 (−11)		
Gln	−60 (−123)	180 (−63)	−60 (−62)	
His	−60 (70)	90 (98)		
Asp	−60 (−160)	0 (15)		
Glu	−60 (−121)	180 (−56)	0 (−73)	
Lys	−60 (−70)	180 (178)	−60 (−70)	−60 (−39)
Arg	−60 (−71)	180 (169)	−60 (−53)	−60 (−65)

[a] Optimized values are indicated in parentheses (see text).

were fixed in an extended conformation (180°, 180°). Each amino acid was hydrated in a sphere of 150 TIP3P water molecules.[48] A spherical solvent boundary potential (SSBP) including a reaction field contribution calculated from the Kirkwood multipolar expansion[29] was used to approximate the influence of the surrounding bulk water.[49] Nonbonded interactions were not truncated at a cutoff distance. The number of water molecules was sufficient to provide more than the first hydration shell of explicit waters for each amino acid side chain. For the individual solute−water systems, the solvent molecules and the side chain were first relaxed with the backbone geometry fixed in an extended conformation for 200 steps of steepest descent energy minimization and then equilibrated for 50 ps using Langevin dynamics simulations in a constant temperature (300 K) with a friction constant corresponding to a relaxation time of 5 ps^{-1} applied to the water oxygen atoms. The geometry of the water molecules was kept fixed using SHAKE,[50] and an integration step of 0.002 ps was used. Optimized side chain conformations are given in Table 1. In the following, we refer to calculations performed with preequilibrated and fixed configurations.

Free Energy Perturbation Calculations. Solvation energies were computed using a modified version of the PERT facility

of CHARMM[51] following standard free energy perturbation techniques.[52,53] The free energy of charging a molecule was calculated for each individual amino acid using 10 windows with the scaled charges λq_i. The configurational sampling was performed using Langevin trajectories generated at 300 K with a friction constant corresponding to a relaxation time of 5 ps^{-1} applied to the water oxygen atoms. Langevin dynamics trajectories of 15 ps were generated for each window, varying λ_i from 0.05 to 0.95 $\pm$ 0.10 by an increment of 0.10. Each trajectory was started from the last configuration of the previous window and equilibrated for 5 ps. Each charging calculation lasted 200 ps corresponding to 18 CPU hours in a SGI R8000. The electrostatic solvation free energy differences were combined using the weighted histogram analysis method (WHAM).[54] This method implies a self-consistent iterative procedure to find the optimal free energy constants F_k generated with a perturbed potential $U(\lambda)$ corresponding to various windows. Assuming that the perturbed potential is given by $U(\lambda) = U_0 + \lambda(U_1 - U_0)$, the free energy constants are obtained from

$$\exp[-F_k/(k_B T)] = \sum_{i=1}^{N_W} \sum_{t=1}^{T_i} \exp[-\lambda_k \Delta U_i(t)/(k_B T)] \times \left[\sum_{j=1}^{N_W} T_j \exp[(F_j - \lambda_j \Delta U_i(t))/(k_B T)]\right]^{-1} \quad (22)$$

where N_W is the number of windows, T_i is the simulation length of the ith window, λ_k is the value of the coupling parameter for the kth window, and $\Delta U_i(t)$ is the potential energy difference $(U_1 - U_0)$ obtained at time t from the ith window. In practice, the WHAM equations are iterated until self-consistency of the constant F_k is achieved. The total free energy change is obtained as the difference between the free energy constants F_k corresponding to $\lambda = 0$ and $\lambda = 1$.

Macroscopic Continuum Electrostatic Calculations. Solvation energies were computed by solving eq 2 using the finite difference algorithm of Klapper et al.,[55] implemented in the PBEQ facility of CHARMM (Beglov, D.; Roux, B.). The dielectric boundary between the solute and the solvent was constructed based on the set of atomic Born radii derived from the average radial charge distribution functions of the explicit solvent around the solute molecules. The dielectric constant of the surrounding continuum was assigned a value of 80. To be consistent with the free energy perturbation with explicit solvent, the dielectric constant in the interior of the solute was assigned a value of 1. The contribution of mobile counterions was not considered in this work. The solute with associated atomic charges was mapped onto a three-dimensional cubic grid. A grid of 20 Å was used with 2, 5, and 10 grid points per Å. The total electrostatic potential was calculated at each point of the grid by solving the Poisson equation (eq 2). The solvent reaction field Ψ_{rf} was obtained by subtracting the Coulomb potential computed in vacuum ($\epsilon = 1$) from the total electrostatic potential computed in a medium representative of water ($\epsilon = 80$) corresponding to the sum of steps 1 and 3 in Scheme 1.

It is important to specify the definition for constructing the dielectric boundary used in the Poisson calculations. In the present calculations, the solute−solvent boundary is constructed as a surface formed of overlapping atomic spheres representing individual atoms of the solute (Figure 3a). A different definition, often employed in numerical Poisson−Boltzmann programs, is to construct the dielectric boundary based on the molecular surface (Figure 3b).[56,57] This definition includes the contact surface and the voids between the solute atoms forming the reentrant surface and is equivalent to the solvent inaccessible volume.[58] In the following, the dielectric boundary was constructed as a surface formed by overlapping spheres, which does not include voids between solute atoms. The influence of the reentrant will be examined.

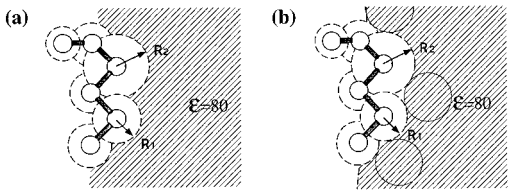

Figure 3. Schematic representation of solute−solvent boundary represented (a) by a surface formed of overlapping atomic spheres and (b) by the molecular surface as defined by Richards.[58] The 1.4 Å probe size is represented by a gray circle of dielectric 80.

IV. Results and Discussion

Radial Distribution Functions and Determination of the Atomic Radii. Average radial solvent charge distribution functions were calculated for all atoms of all the amino acids except hydrogens from a 50 ps Langevin trajectory. Figures 4−10 show representative radial solvent charge distribution functions for a few selected atom types. Distribution functions of backbone atoms of Gly (N, CA, C, and O) are displayed in Figure 4. Figure 5 shows distribution functions for nonpolar atoms CA of Gly, Ala, Arg, Asn, and Trp. Figures 6 and 7 show distribution functions for atoms forming Phe and Trp rings, respectively. Distribution functions for polar atoms (oxygen OG*, OH) of Ser, Tyr, and Thr are plotted in Figure 8. Finally, the distribution functions for negatively (OD* and OE* of Asp) and positively (NH*, NE, NZ of Arg and Lys) charged atoms are shown in Figures 9 and 10, respectively. Despite the increasing noise at large distance, the structure of the solvent charge distribution is apparent. The solvation structure around apolar, polar, or charged atoms differs as shown by the differences in the solvent radial charge distribution functions. The solvent charge distribution function around apolar atoms is broad and contrasts with those of polar and charged atoms, which are sharply peaked. As expected, there is a peak of net positive solvent charge density, corresponding to the water hydrogen atoms, around negatively charged solute atoms. Correspondingly, there is peak of net negative solvent charge density of water oxygen atoms around positively charged solute atoms. Comparison of the shape of the distribution in the case of negatively and positively charged atoms reveals that the structure of the solvent also differs with the sign of the charge of a given atom. Such behavior is consistent with previous experimental results on proteins[59] and with Monte Carlo simulations on small molecules.[60,61] Similarly, it is reflected on simple monatomic ions such as Cl^- and K^+ (see Figure 1b above).

The set of atomic radii was developed and optimized on the basis of the average radial solvent charge distribution functions. The initial value of all the radii was directly taken from the distance corresponding to zero before the first peak position of the solvent charge distribution function. The atomic radii were then refined to quantitatively reproduce the results from free energy simulations with explicit water molecules. Table 2 lists the optimized atomic Born radii for all atoms types of the standard amino acids. The optimized radii, indicated in the figures by an arrow, correspond closely to the initial values. The solvation structure around the backbone atoms of the Gly tripeptide was used to determine the radii for the backbone atoms (CAY, CY, N, C, O, NT, and CAT in Figure 2b) and applied to all amino acids regardless of the side chain grouping.

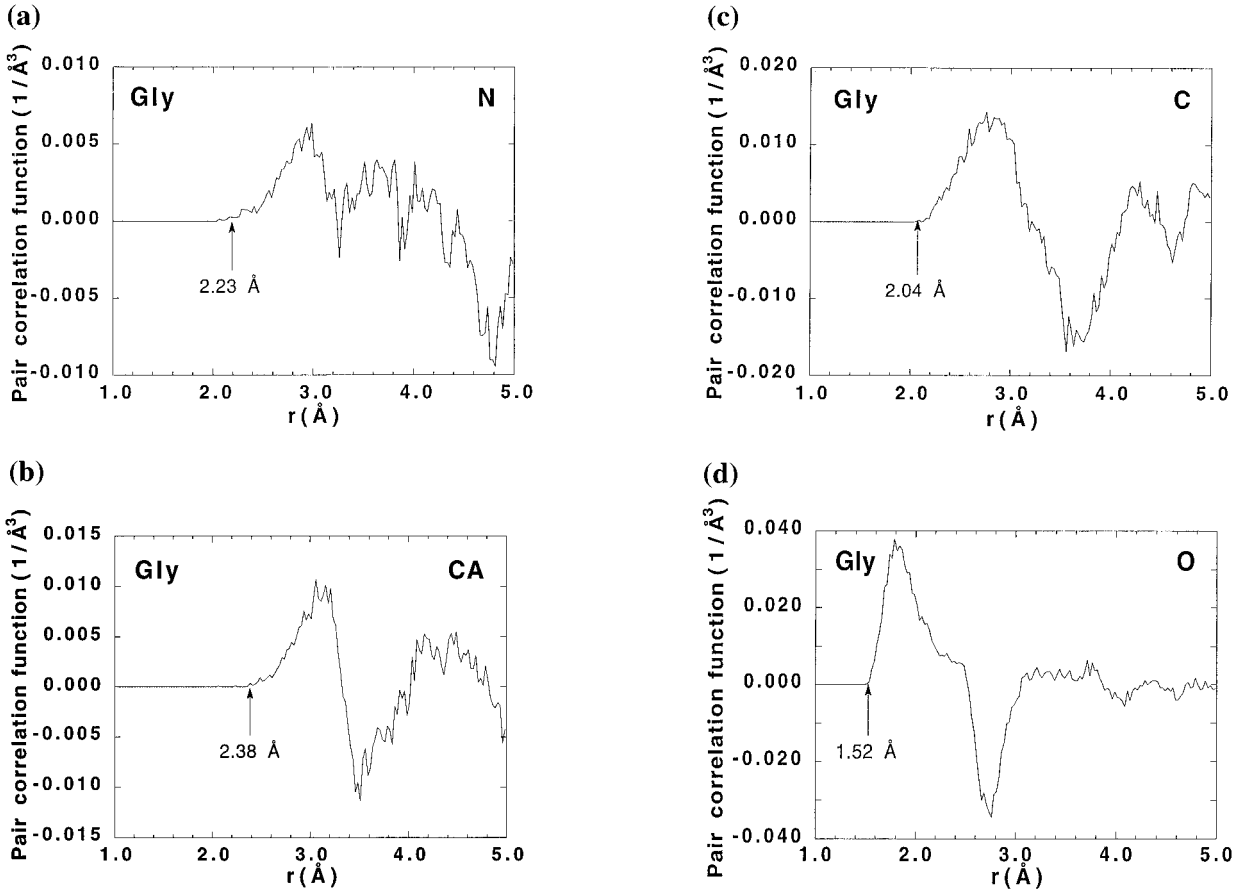

Figure 4. Average radial charge distribution functions are plotted versus distance in Å for the distribution of water hydrogen and oxygen charges around the backbone atoms of Gly: N, CA, C and O atom types.

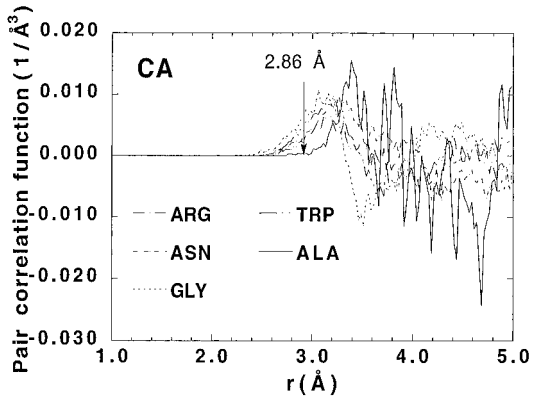

Figure 5. Average radial charge distribution functions are plotted versus distance in Å for the distribution of water hydrogen and oxygen charges around CA of Gly, Ala, Arg, Asn, and Trp.

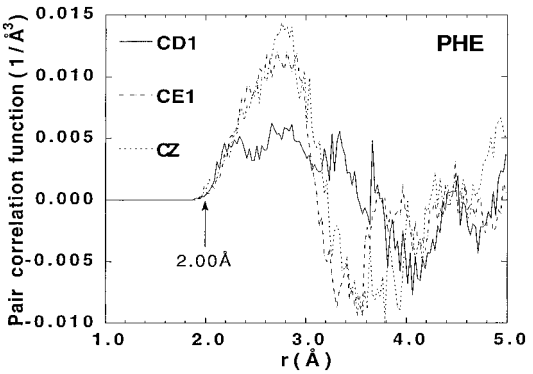

Figure 6. Average radial charge distribution functions are plotted versus distance in Å for the distribution of water hydrogen and oxygen charges around ring atoms of Phe.

Average radial charge distribution functions around CA atoms plotted in Figure 5 indicate that the Born radius for CA of Gly is smaller then all other CA radii. As a consequence, the atomic Born radius for CA of the backbone found for Ala was assigned to all amino acids excepted for Gly and Pro as shown in Table 2. The generally broad distribution around CA of Gly shown in Figure 5 appears to be different from those around CA of Ala. This difference may be attributed to the fact that the amino acid environment of CA is influenced by the methyl group side chain, which is absent for Gly. The solvation structure around atoms is modulated by the side chain groups and the conformation of the amino acid, also seen in the radial distribution functions for Arg, Asn, and Trp. The atomic radius for CB found for Ala was assigned to all tripeptides except for Pro. Based on the distribution functions, the water structure near identical groups was found to be very similar, and as a consequence, the same atomic Born radius was attributed to identical groups regardless of the atom types for the sake of simplicity. For example, atoms forming carboxylate groups of Asp and Glu were assigned an identical radius (CG in Asp is identical to those of CD in Glu, and the oxygen atoms OD* in Asp are identical to atoms OE* in Glu). Based on the water structure around atoms forming the cyclic side chain of Phe shown in Figure 6, identical radii were assigned to all atoms except CG whose value is kept identical to those of all CG (see Table 2). The radii of the Trp ring were assigned identical values (see Figure 7). As shown in Figure 8, the water structures around oxygen atoms of Ser, Thr, and Tyr are very similar. Although the radii for Thr and Ser oxygen atoms were considered identical, it was necessary to increase the oxygen radii for Tyr to obtain the electrostatic contribution calculated

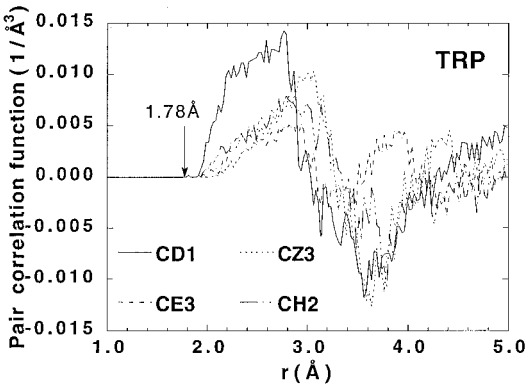

Figure 7. Average radial charge distribution functions are plotted versus distance in Å for the distribution of water hydrogen and oxygen charges around ring atoms of Trp.

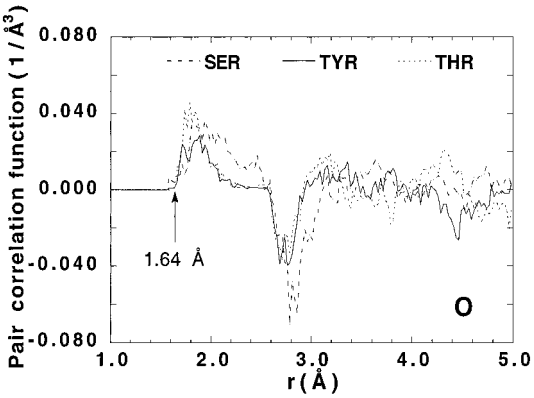

Figure 8. Average radial charge distribution functions are plotted versus distance in Å for the distribution of water hydrogen and oxygen charges around oxygen atoms: OG of Ser, OH, of Tyr, and OG1 of Thr.

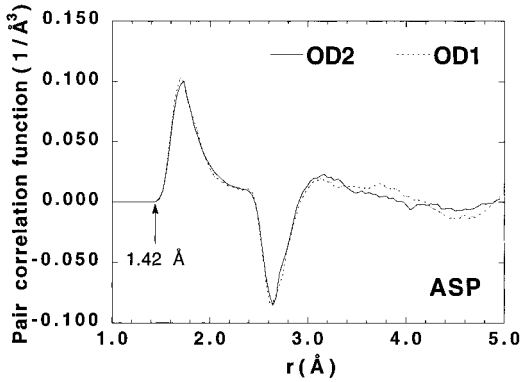

Figure 9. Average radial charge distribution functions are plotted versus distance in Å for the distribution of water hydrogen and oxygen charges around negatively charged oxygen atoms: OG and OE of Asp (results for Glu were identical and are not shown for the sake of clarity).

with free energy perturbation methods. As shown in Figure 9, a similar behavior was found for the water structure around negatively charged oxygen atoms (OD* and OE*) in the Asp carboxylate group (results for Glu are identical and are not shown for the sake of clarity). Identical atomic radii were assigned to NH1, NH2, and NE from Arg and to NZ from Lys, since their solvation structure is similar, as shown in Figure 10.

Electrostatic Solvation Free Energy. Table 3 gives the results obtained for the standard 20 amino acids modeled by *N*-acetyl-X-*N*′-methylamide using free energy perturbation techniques and molecular dynamics simulations (WHAM column). Amino acids with nonpolar side chains have associated

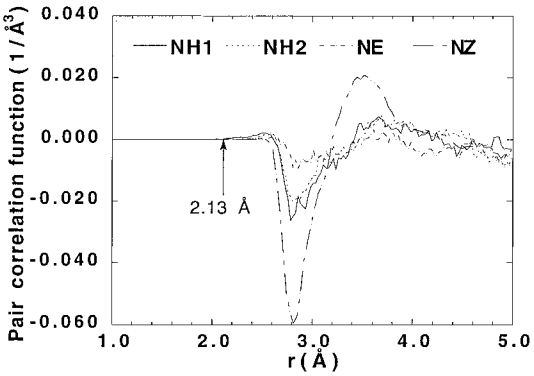

Figure 10. Average radial charge distribution functions are plotted versus distance in Å for the distribution of water hydrogen and oxygen charges around NH* and NE of Arg and NZ of Lys.

TABLE 2: Atomic Born Radii Derived from Solvent Electrostatic Charge Distribution Tested with Free Energy Perturbation Methods in an Explicit Solvent[a]

atom	radius (Å)	
	Backbone	
C	2.04	carbonyl C, peptide backbone
O	1.52	carbonyl oxygen
	2.23	peptide nitrogen
CA	2.86	all CA except Gly
CA	2.38	Gly only
	Hydrogens	
H*	0.00	all hydrogens
	Side Chains	
CB	2.67	all residues
CG*	2.46	Val, Ile, Arg, Lys, Met, Phe, Thr, Trp, Gln, Glu
CD*	2.44	Ile, Leu, Arg, Lys
CD, CG	1.98	Asp, Glu, Asn, Gln
CB, CG, CD	1.98	Pro only
CE*, CD*, CZ,	2.00	Tyr, Phe rings
CE*, CD*, CZ*, CH2	1.78	Trp ring only
CE	2.10	Met only
CZ, CE	2.80	Arg, Lys
OE*, OD*	1.42	Glu, Asp, Asn, Gln
OG*	1.64	Ser, Thr
OH	1.85	Tyr only
NH*, NE, NZ	2.13	Arg, Lys
NE2, ND2	2.15	Gln, Asn
NE2, ND1	2.31	His only
NE1	2.40	Trp
S*	2.00	Met, Cys

[a] Patches N-term and C-term CAT, CAY: 2.06 Å. CY: 2.04 Å. OY: 1.52 Å. NT: 2.23 Å. * refers to a wild card character.

electrostatic free energy contributions of about −17.9 to −10.4 kcal/mol and neutral polar groups of about −25.7 to −15.5 kcal/mol, modest in comparison with the large electrostatic free energy contributions of ammonium and carboxylate groups of about −91.9 to −66.0 kcal/mol. Free energy perturbation results obtained using standard TP and TI techniques were very similar (not shown). Results obtained with standard techniques and combined with the WHAM method differed by 0.02 kcal/mol or less for the ensemble of the 20 molecules, indicating that an adequate conformational sampling has been performed and that convergence has been achieved.[62] The uncertainty of the free energy perturbation results is estimated to be about 0.5 kcal/mol. The validity of one important assumption of the continuum electrostatic theory that the water polar solvent responds linearly to changes in the electrostatic field can be examined on a microscopic level (ref 63, and references therein). The ratio $\Delta G_{elec}(\lambda)/\Delta G_{elec}(\lambda = 1)$, calculated for different amino acids−water systems, is shown in Figure 11. The result of the thermodynamic integration in the case of a nonpolar (Ala) and charged amino acids (Asp and Lys) is shown in Figure 11. It is

TABLE 3: Electrostatic Contribution to Solvation Free Energy for All Standard Amino Acids Using a Continuum and an Excplicit Model of the Solvent

		Poisson		
residues	WHAM	*a*	*b*	*c*
		Nonpolar Groups		
Gly	−13.3	−13.3	−13.2	−13.3
Ala	−11.9	−12.9	−12.0	−12.1
Val	−10.4	−11.3	−10.5	−10.5
Leu	−11.4	−13.0	−11.8	−11.6
Ile	−10.8	−11.3	−10.4	−10.4
Pro	−16.5	−15.3	−16.4	−16.5
Phe	−14.6	−15.6	−14.7	−14.0
Trp	−17.9	−19.6	−17.8	−16.3
Met	−11.2	−12.3	−11.1	−11.2
		Neutral Polar Groups		
Ser	−19.7	−21.7	−19.6	−20.0
Thr	−18.1	−20.2	−17.9	−18.4
Cys	−15.5	−16.6	−15.4	−15.4
Tyr	−19.0	−21.6	−19.1	−19.1
Asn	−20.8	−22.3	−20.8	−20.9
Gln	−16.7	−16.7	−16.6	−16.6
His	−25.7	−26.9	−25.9	−24.4
		Charged Polar Groups		
Asp	−91.9	−81.5	−91.0	−91.5
Glu	−87.8	−78.0	−88.3	−87.5
Lys	−72.9	−87.8	−72.9	−72.2
Arg	−66.0	−81.6	−66.3	−67.0

[a] Atomic radii from PARM22.[44] [b] Atomic Born radii. The solute−solvent boundary is defined as a surface formed of overlapping atomic spheres. [c] Atomic Born radii increased by 2%. The dielectric boundary is defined as the molecular surface.

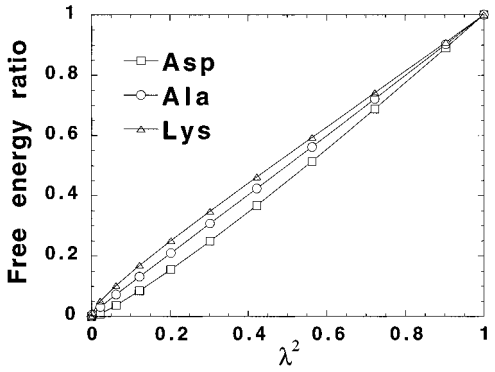

Figure 11. Free energy ratio $\Delta G_{elec}(\lambda)/\Delta G_{elec}(1)$ is plotted versus λ^2 for nonpolar Ala and for charged Asp and Lys residues.

observed that the response of the free energy during the charging procedure is nearly linear. A slight deviation appeared to positively and negatively charged amino acids (Figure 11). As found in previous work, a linear reponse is generally satisfied for neutral and nonpolar molecules.[63] Deviations from linear reponse in the case of ionic solutes are mainly due to the asymmetry of the charge distribution in the water molecules.[63]

As shown in Table 4, the electrostatic contribution to the solvation free energy calculated in the continuum approach, with the atomic Born radii previously defined, reproduces quite well the results from free energy perturbation molecular dynamics simulations. Electrostatic contributions to the solvation free energy obtained from the continuum model (Poisson column) are independent of the hydrogen radii up to a maximum value for hydrogen atoms whose radii are so small that they are completely enclosed in the atomic sphere of another atom. For example, the atomic Born radii of the backbone nitrogen is 2.23 Å (see Table 2). Since the N−H bond length is 1.0 Å, the hydrogen radius can vary between 0.0 and 1.23 Å without having an effect on the solute−solvent boundary. Different

TABLE 4: Electrostatic Contribution to Solvation Free Energy of All Standard Amino Acids as a Function of the Grid Size Used in Poisson Calculations and of the Hydrogen Radius

		Poisson					
		r_H (Å)[a]		grid size[b]			
residues	WHAM	1.0	0.6	10-200	5-100	2-40	2-80
		Nonpolar Groups					
Gly	−13.3	−13.2	−13.2	−12.9	−13.2	−14.1	−14.1
Ala	−11.9	−12.0	−12.0	−11.8	−12.0	−12.4	−12.4
Val	−10.4	−10.5	−12.5	−10.3	−10.5	−11.0	−11.0
Leu	−11.4	−11.8	−11.8	−11.6	−11.8	−12.9	−12.9
Ile	−10.8	−10.4	−10.4	−10.2	−10.4	−11.0	−11.0
Pro	−16.5	−16.3	−16.4	−16.2	−16.4	−16.8	−16.8
Phe	−14.6	−15.3	−15.3	−15.1	−14.7	−16.0	−16.0
Trp	−17.9	−17.1	−17.8	−17.5	−17.8	−18.9	−18.9
Met	−11.2	−11.1	−11.1	−10.9	−11.1	−12.1	−12.1
		Neutral Polar Groups					
Ser	−19.7	−18.7	−19.6	−19.2	−19.6	−21.2	−21.2
Thr	−18.1	−17.3	−17.9	−17.6	−17.9	−19.1	−19.1
Cys	−15.5	−15.0	−15.4	−15.2	−15.4	−15.8	−15.8
Tyr	−19.0	−19.3	−19.6	−19.4	−19.1	−21.2	−21.2
Asn	−20.8	−20.8	−20.8	−20.5	−20.8	−22.7	−22.7
Gln	−16.7	−16.6	−16.6	−16.3	−16.6	−18.7	−18.7
His	−25.7	−20.3	−21.7	−24.7	−25.9	−24.7	−24.7
		Charged Polar Groups					
Asp	−91.9	−91.0	−91.0	−90.3	−91.0	−95.9	−95.9
Glu	−87.8	−88.3	−88.3	−87.6	−88.3	−90.7	−90.7
Lys	−72.9	−72.9	−72.9	−72.4	−72.9	−73.7	−73.7
Arg	−66.0	−66.3	−66.3	−65.8	−66.3	−68.9	−68.9

[a] A grid size of 20 Å was used with 5 grid points/Å. $r_H = 0.0$ Å. [b] The number of grid points per Å and the total number of grid points, respectively.

values for the unique hydrogen radius identical for all hydrogen atoms, were tested up to 1.0 Å and indicated that the free energies of solvation of the 20 amino acids conformations considered here were independent of the hydrogen radius up to 0.5 Å except for Phe, Tyr, and His (Table 4). For the sake of simplicity, the atomic radius of the hydrogen was set to zero. The influence of increasing all atomic Born radii on the continuum electrostatic free energies was tested by increasing all atomic Born radii by 1%. These results indicated an increase in average electrostatic free energy of solvation of nonpolar groups by 0.3 kcal/mol, neutral polar groups by 0.4 kcal/mol, and charged polar groups by 1 kcal/mol.

To evaluate the contribution of the voids inaccessible to the water to the solvation free energies, the boundary between the dielectrics was also defined as the molecular surface (including the reentrant). Results (not shown) indicated that this change in the solute−solvent boundary increases at most by 7% of the electrostatic contribution to solvation free energies of the amino acids. In order to recover the fit to the free energy perturbation results for all amino acids with the molecular definition, the atomic radii previously optimized (Table 2) needed to be decreased by 2%. The corrected electrostatic free energies obtained from this radii deviate from the free energy perturbation values by a maximum of only 1.6 kcal/mol and on average by 0.36 kcal/mol (Table 4). The construction of the dielectric boundary around the solute based on the molecular surface is more time-consuming computationally. However, it is important to use the molecular surface, since voids between the solute atoms contribute to create spurious cavities of solvent dielectric in the interior of proteins. For this reason it will be important to consider the molecular surface, since it reproduces the limit between the polarizable and nonpolarizable medium.

The influence of the spacing of the lattice points on the results was examined for a fixed grid size of 20 Å with 2 and 10 grid

points/Å. From Table 4, these tests suggested that the continuum electrostatic free energy of solvation decreases by less than 1 kcal/mol when improving the accuracy of the calculations from 2 to 5 grid points/Å. Improving the grid spacing from 5 to 10 grid points/Å increases the ensemble of free energies of solvation by less than 0.3 kcal/mol, whereas the computational cost is almost 30 times higher. The influence of the size of the grid was tested with a spacing of the lattice points of 5 grid points/Å to investigate the effect of varying the distance from the solute to the grid boundaries. These tests suggested that results do not differ when calculations are performed in a 20 or 80 Å grid size with 5 grid points/Å. The convergence of the electrostatic free energy was tested with respect to the grid spacing. The molecule was translated by a half of the gris spacing in all directions, and the electrostatic free energy of solvation was calculated at each point to estimate the translational averaged error. These tests indicated that the translational averaged error is estimated to be ±0.03 kcal/mol with a spacing of the lattice points of 5 grid points/Å and a 20 Å grid size.

V. Summary and Conclusion

Detailed atomic molecular dynamics simulations were used to develop a new set of "atomic Born radii" for the 20 standard amino acids for the purpose of defining the dielectric boundary in continuum electrostatic calculations. In a first step, the atomic radii were obtained from an analysis of the average solvent charge distribution functions and used to define the solute−solvent dielectric boundary. The atomic radii were then refined to quantitatively reproduce the results from free energy simulations with explicit water molecules. The electrostatic free energy of solvation obtained using free energy perturbation simulations is reproduced accurately within the macroscopic model by the final set of atomic Born radii. The new set of atomic Born radii for all standard amino acids to be used in conjunction with the all-hydrogen PARM22 force field for which it was derived is the main result of the paper.

The approach used here can be applied to develop atomic radii for any molecular solute on the basis of simulations with explicit solvent molecules. Although the initial parametrization was straightforward, the optimization involved some compromises; e.g., the same atomic radius was assigned to identical chemical groups regardless of the atom types. The final set of radii results in a good agreement between microscopic and macroscopic calculations. The agreement between the two approaches ensures that the two different descriptions yield a consistent estimate of the electrostatic contribution to the solvation free energy. The ability to compare both microscopic and macroscopic models in simple systems provides a sound basis for applying macroscopic approaches to a wide range of biological problems. Testing new ideas becomes simpler and less time-consuming compared to molecular dynamics simulations in which water molecules are included explicitly.

To estimate the total free energy of solvation for the 20 amino acids, it is necessary to account for the overall solvation free energy. This requires calculating the nonpolar contribution to the solvation free energy within a continuum approximation. Future developments for improving the description of solvation will involve the treatment of the nonpolar aspect of solvation. This will allow comparison with experimental values of the solvation free energy of small peptides.[64,65] The accurate estimation of the solvation free energy should lead to a better insight of important biological processes involving protein folding, conformational equilibrium, association of biomolecules, and protein membrane interactions.

Acknowledgment. This research was supported by NSERC and by MRC.

References and Notes

(1) Privalov, P. L.; Makhatadze, G. I. *J. Mol. Biol.* **1993**, *232*, 660.
(2) Nicholls, A.; Sharp, K.; Honig, B. *Proteins* **1991**, *11*, 281.
(3) Cabani, S.; Gianni, P.; Mollica, V.; Lepori, L. *J. Solution Chem.* **1981**, *10*, 563.
(4) Mohan, V.; Davis, M. E.; McCammon, J. A.; Pettitt, B. M. *J. Phys. Chem.* **1992**, *96*, 6428.
(5) McCammon, J. A.; Straatsma, T. P. *Annu. Rev. Phys. Chem.* **1992**, *43*, 407.
(6) Boresch, S.; Archontis, G.; Karplus, M. *Proteins* **1994**, *20*, 25.
(7) Brooks, C. L., III; Karplus, M.; Pettitt, B. M. *Proteins. A theoretical perspective of dynamics, structure and thermodynamics*; John Wiley & Sons: New York, 1988.
(8) Tobias, D. J.; Mertz, J. E.; Brooks, C. L., III. *Biochemistry* **1991**, *30*, 6054.
(9) Tobias, D. J.; Brooks, C. L., III. *Biochemistry* **1991**, *30*, 6059.
(10) Gao, J.; Kuczera, K.; Tidor, B.; Karplus, M. *Science* **1989**, *244*, 1069.
(11) Kollman, P. *Chem. Rev.* **1993**, *93*, 2395.
(12) Jorgensen, W. L.; Gao, J. *J. Am. Chem. Soc.* **1988**, *110*, 4212.
(13) Postma, J. P.; Berendsen, H. C.; Haak, J. R. *Faraday Symp. Chem. Soc.* **1982**, *17*, 55.
(14) Mazor, M.; Pettitt, B. M. *Mol. Simul.* **1991**, *6*, 1.
(15) Mitchell, M. J.; McCammon, J. A. *J. Comput. Chem.* **1991**, *12*, 271.
(16) Pearlman, D. A.; Kollman, P. A. *J. Chem. Phys.* **1991**, *94*, 4532.
(17) Chotia, C. *Nature* **1974**, *248*, 338.
(18) Fauchère, J.-L.; Plíska, V. *Eur. J. Med. Chem.* **1983**, *18*, 369.
(19) Eisenberg, D.; McLachlan, A. D. *Nature* **1986**, *319*, 199.
(20) Ooi, T.; Oobatake, M.; Némethy, G.; Scheraga, H. A. *Proc. Natl. Acad. Sci. U.S.A.* **1987**, *84*, 3086.
(21) Wesson, L.; Eisenberg, D. *Protein Sci.* **1992**, *1*, 227.
(22) Wimley, C. W.; Creamer, T. P.; White, S. H. *Biochemistry* **1996**, *35*, 5109.
(23) Simonson, T.; Brunger, A. *J. Phys. Chem.* **1994**, *98*, 4683.
(24) Sitkoff, D.; Sharp, K. A.; Honig, B. *J. Phys. Chem.* **1994**, *98*, 1978.
(25) Sitkoff, D.; Ben-Tal, N.; Honig, B. *J. Phys. Chem.* **1996**, *100*, 2744.
(26) Ben-Tal, N.; Nicholls, A.; Honig, B. *Biophys. J.* **1996**, *70*, 1803.
(27) Honig, B.; Sharp, K.; Yang, A.-S. *J. Phys. Chem.* **1993**, *97*, 1101.
(28) Born, M. *Z. Phys.* **1920**, *1*, 45.
(29) Kirkwood, J. G. *J. Chem. Phys.* **1934**, *2*, 351.
(30) Warwicker, J.; Watson, H. C. *J. Mol. Biol.* **1982**, *157*, 671.
(31) Honig, B.; Nicholls, A. *Science* **1995**, *268*, 1144.
(32) Zauhar, R. J.; Morgan, R. S. *J. Mol. Biol.* **1985**, *186*, 815.
(33) Jayaram, B.; Fine, R.; Sharp, K.; Honig, B. *J. Phys. Chem.* **1989**, *93*, 4320.
(34) Hirata, F.; Redfern, P.; Levy, R. M. *Int. J. Quantum Chem., Quantum Biol. Symp.* **1988**, *15*, 179.
(35) Roux, B.; Yu, H.-A.; Karplus, M. *J. Phys. Chem.* **1990**, *94*, 4683.
(36) Rashin, A. A.; Honig, B. *J. Phys. Chem.* **1985**, *89*, 5588.
(37) Lim, C.; Bashford, D.; Karplus, M. *J. Phys. Chem.* **1991**, *95*, 5610.
(38) Jorgensen, W. L.; Tirado-Rives, J. *J. Am. Chem. Soc.* **1988**, *110*, 1657.
(39) Weiner, S. J.; Kollman, P. A.; Case, U. C.; Ghio, C.; Alagona, G.; Profeta, S.; Weiner, P. *J. Am. Chem. Soc.* **1973**, *106*, 765.
(40) Jean-Charles, A.; Nicholls, A.; Sharp, K.; Honig, B.; Tempczyk, A.; Hendrickson, T. F.; Still, C. *J. Am. Chem. Soc.* **1991**, *113*, 1454.
(41) Ewing, T. J. A.; Lybrand, T. P. *J. Phys. Chem.* **1994**, *98*, 1748.
(42) Marrone, T. J.; Gilson, M. K.; McCammon, J. A. *J. Phys. Chem.* **1996**, *100*, 1439.
(43) Jackson, J. D. *Classical electrodynamics*; John Wiley & Sons: New York, 1962.
(44) Roux, B. *Biophys. J.* **1996**, *71*, 3177.
(45) Beglov, D.; Roux, B. *J. Chem. Phys.* **1996**, *104*, 8678.
(46) Mackerell, A. D., Jr.; Bashford, D.; Bellot, M.; Dunbrack, R. L.; Field, M. J.; Fischer, S.; Gao, J.; Guo, H.; Joseph, D.; Ha, S.; Kuchnir, L.; Kuczera, K.; Lau, F. T. K.; Mattos, C.; Michnick, S.; Nguyen, D. T.; Ngo, T.; Prodhom, B.; Roux, B.; Schlenkrich, B.; Smith, J.; Stote, R.; Straub, J.; Wiorkiewicz-Kuczera, J.; Karplus, M. *Biophys. J.* **1992**, *61*, A143.
(47) Dunbrack, R. L.; Karplus, M. *J. Mol. Biol.* **1993**, *230*, 543.
(48) Jorgensen, W. L.; Chandrasekhar, J.; Madura, J. D.; Impey, R. W.; Klein, M. L. *J. Chem. Phys.* **1983**, *79*, 926.
(49) Beglov, D.; Roux, B. *J. Chem. Phys.* **1994**, *100*, 9050.
(50) Ryckaert, J. P.; Ciccotti, G.; Berendsen, H. J. C. *J. Comput. Phys.* **1977**, *23*, 327.
(51) Brooks, B. R.; Bruccoleri, R. E.; Olafson, B. D.; States, D. J.; Swaminathan, S.; Karplus, M. *J. Comput. Chem.* **1983**, *4*, 187.
(52) Straatsma, T. P.; Berendsen, H. J. C.; Postma, J. P. M. *J. Chem. Phys.* **1986**, *85*, 6720.

(53) Straatsma, T. P.; Berendsen, H. J. C.; Postma, J. P. M. *J. Chem. Phys.* **1988**, *89*, 5876.
(54) Kumar, S.; Bouzida, D.; Swendsen, R. H.; Kollman, P. A.; Rosenberg, J. M. *J. Comput. Chem.* **1992**, *13*, 1011.
(55) Klapper, I.; Hagstrom, R.; Fine, R.; Sharp, K.; Honig, B. *Proteins* **1986**, *1*, 47.
(56) Davis, M. E.; Madura, J. D.; Luty, B. A. *Comput. Phys. Commun.* **1991**, *62*, 187.
(57) Gilson, M. K.; Honig, B. *Proteins* **1988**, *3*, 32.
(58) Richards, F. M. *Annu. Rev. Biophys. Bioeng.* **1977**, *6*, 151.
(59) Jiang, J.-S.; Brunger, A. *J. Mol. Biol.* **1994**, *243*, 100.
(60) Berendsen, H. J. C. Postma, J. P. M., van Gunsteren, W. F., Hermans, J. B. Pullman Eds.; *XXX*; Reidel: Dordrecht, 1981.
(61) Mezei, M.; Mehrotra, P. K.; Beveridge, D. L. *J. Am. Chem. Soc.* **1985**, *107*, 2239.
(62) Roux, B. *Comput. Phys. Commun.* **1995**, *91*, 275.
(63) Åqvist, J.; Hansson, T. *J. Phys. Chem.* **1996**, *100*, 9512.
(64) Wolfenden, R.; Andersson, L.; Cullis, P. M.; Southgate, C. C. B. *Biochemistry* **1981**, *20*, 849.
(65) Radzicka, A.; Wolfenden, R. *Biochemistry* **1988**, *27*, 1664.